J Mater Sci (2009) 44:745–753
DOI 10.1007/s10853-008-3157-1

Phase-field simulation of directional solidification of a binary alloy under different boundary heat flux conditions

Jinjun Tang · Xiang Xue

Received: 9 September 2008 / Accepted: 3 December 2008 / Published online: 27 December 2008

Abstract Complicated morphologies of directional solidification structures attract a lot of theoretical studies and commercial uses. As known, the boundary heat flux has an important significance to the microstructures of directional solidification. In this article, the interface evolution of directional solidification with different boundary heat fluxes is discussed. In this study, only one interface has heat flow, and Neumann boundary conditions are imposed at the other three interfaces. From the calculated results, it is found that different heat fluxes cause different microstructures in the directional solidification. When the heat flux equal to 18 W/cm^2, the growth of lengthways side branches is accelerated and the growth of transverse side branches is restrained. At the same time, there is dendritic remelting in the calculating domain. When the heat flux equal to 36 W/cm^2, the growth of the transverse side branches and the growth of the lengthways side branches compete with each other. When the heat flux equal to 90 or 180 W/cm^2, the growth of transverse side branches absolutely dominates. The temperature field of dendritic growth is also analyzed and the relation between heat flux and temperature field is found.

Introduction

The phase-field model has been used for computing the solidification morphologies to avoid the explicit boundary tracking needed to solve the classical sharp interface model. An auxiliary variable, Φ, is introduced to indicate the phases. Φ makes a continuous transition over a thin diffuse interface from its value 0 in bulk solid to 1 in bulk liquid. Alloy phase-field models have been formulated by many scholars in the last 15 years. Wheeler et al. [1, 2] introduced the phase-field model of binary alloy firstly, which is called WBM model. This model was developed by Wheeler and Boettinger [3–5]. In 1999, Kim et al. [6, 7] gave another phase-field model by adopting thin interface limit. Recently, Boettinger et al. [8] generalized the WBM model, and gave a model fitting for regular alloy.

The directional solidification technology offers an effective material preparation and forming method, and it is extensively applied in practical fields. So, the theoretical study of directional solidification is a central theme of solidification researches. Kim and Kim [9] simulated a rapid directional solidification under a constant thermal gradient by a new phase-field model. Diepers et al. [10] described numerical experiments to investigate the selection of primary dendritic spacing and transient condition. Bi and Sekerka [11] studied the directional solidification and concentrate on the transition between a planar interface and steady shallow cells near the onset of morphological instability at low growth speeds. Guo et al. [12] simulated the structure evolution of $Ti_{55}Al_{45}$ alloy during directional solidification. Costa Filho et al. [13] studied the wavelength selection in two dimensions. Lan et al. [14–16] studied the morphological instability during directional solidification of a succinonitrile/acetone alloy. Singer et al. [17] determined the morphology diagrams in two and three dimensions for two different phase-field models. Mathis Plapp [18] investigated three-dimensional phase-field simulation of directional solidification. However, there are few researchers studying the effect of heat flux on

J. Tang (✉) · X. Xue
School of Materials Science and Engineering, Harbin Institute of Technology, P.O. Box 434, Harbin 150001, People's Republic of China
e-mail: jinjun.tang@163.com

X. Xue
e-mail: xxue@hit.edu.cn

microstructures. In this article, the boundary heat flux is investigated as a main subject. The microstructure of directional solidification is obtained by changing the boundary heat flux high or low. In the non-isothermal simulation, the temperature field is the uppermost factor affecting dendritic growth. Therefore the temperature-field data are also given and analyzed in this article.

Mathematical model and numerical issues

The phase-field model is given in Refs. [4, 8], and the main equations are given as follows.

$$\frac{\partial \Phi}{\partial t} = -M_\Phi \frac{\partial F(c,\Phi,T)}{\partial \Phi}, \tag{1}$$

$$\frac{\partial c}{\partial t} = \nabla \cdot \left[M_c c(1-c) \nabla \left(\frac{\partial F(c,\Phi,T)}{\partial c} \right) \right], \tag{2}$$

$$\frac{\partial T}{\partial t} = D_T \nabla^2 T + \frac{(1-c)L_\mathrm{A} + cL_\mathrm{B}}{C_P} \sum \bar{A} \cdot \frac{\partial \Phi}{\partial t}, \tag{3}$$

$$F(c,\Phi,T) = \int_V [f(c,\Phi,T) + \frac{\varepsilon^2}{2} |\nabla \Phi|^2] \mathrm{d}V, \tag{4}$$

$$\begin{aligned} f(c,\Phi,T) = {} & (1-c) f_\mathrm{A}(\Phi,T) + c f_\mathrm{B}(\Phi,T) \\ & + \frac{R_\mathrm{g} T}{v_\mathrm{m}} [c \ln c + (1-c)\ln(1-c)] \\ & + c(1-c)\{\Omega_\mathrm{L}[1-p(\Phi)] + \Omega_\mathrm{s} p(\Phi)\}, \end{aligned} \tag{5}$$

$$f_\mathrm{A}(\Phi,T) = W_\mathrm{A} g(\Phi) + L_\mathrm{A} \frac{T_\mathrm{m}^\mathrm{A} - T}{T_\mathrm{m}^\mathrm{A}} p(\Phi), \tag{6}$$

$$f_\mathrm{B}(\Phi,T) = W_\mathrm{B} g(\Phi) + L_\mathrm{B} \frac{T_\mathrm{m}^\mathrm{B} - T}{T_\mathrm{m}^\mathrm{B}} p(\Phi), \tag{7}$$

$$g(\Phi) = \Phi^2(1-\Phi)^2, \quad p(\Phi) = \Phi^3\left(10 - 15\Phi + 6\Phi^2\right), \tag{8}$$

$$M_\mathrm{C} = \frac{D_\mathrm{S} + p(\Phi)(D_\mathrm{L} - D_\mathrm{S})}{R_\mathrm{g} T / v_\mathrm{m}}, \tag{9}$$

$$M_\Phi = (1-c)M_\mathrm{A} + cM_\mathrm{B}, \tag{10}$$

$$\varepsilon = \varepsilon_0(1 + r\cos(k\theta)), \tag{11}$$

M_Φ and M_C are phase-field kinetic parameter. M_A, M_B, W_A, W_B, and ϵ_0 are parameters of the phase-field model, given by

$$M_\mathrm{A} = \frac{T_\mathrm{m}^\mathrm{A} \beta^\mathrm{A}}{6 L^\mathrm{A} \delta^\mathrm{A}}, \quad M_\mathrm{B} = \frac{T_\mathrm{m}^\mathrm{B} \beta^\mathrm{B}}{6 L^\mathrm{B} \delta^\mathrm{B}}, \tag{12}$$

$$W_\mathrm{A} = \frac{3\sigma^\mathrm{A}}{\delta^\mathrm{A}}, \quad W_\mathrm{B} = \frac{3\sigma^\mathrm{B}}{\delta^\mathrm{B}}, \tag{13}$$

$$\varepsilon_0^2 = 6\sigma^\mathrm{A}\delta^\mathrm{A}, \tag{14}$$

where Φ is the phase field taking a value of 0 in the solid and 1 in the liquid, c is the solute concentration, and T is the temperature. F(c, Φ, T) is the volume-free energy, and $f(c, \Phi, T)$ is the density of free energy. $f_\mathrm{A}(\Phi, T)$ and $f_\mathrm{B}(\Phi, T)$ are the free energy density of the pure components A and B. W_A and W_B are the energy barrier of the pure components A and B. D_T is the heat conductivity, R_g is the gas constant, and v_m is the molar volume. D_L and D_S are the diffusivities in liquid and solid, respectively. σ^A and σ^B are the interfacial energy of pure materials A and B, respectively. β^A and β^B are the kinetic coefficients of pure materials A and B, respectively. T_m^AandT_m^B are the melting points of pure materials A and B, respectively, L^A and L^B are the latent heat of pure materials A and B, respectively, and δ^A and δ^B are the interface thickness of pure materials A and B, respectively. r, k, and θ are the parameters of anisotropic property. Ω_L and Ω_S are the parameters of regular solution, and it is ideal solution when both are equal to 0. In our simulations, Ni–Cu alloy is used, which is an ideal solution, and Ω_L and Ω_S both are equal to 0. Because the thermal diffusivity is generally hundreds of times higher than solute diffusivity, the solution procedure of Eq. 3 should be based on macroscopical lattice. The macroscopical lattice of temperature field is 10 times of microscopic lattice in this article. $\bar{A}$ is the area ratio of microscopic-to-macroscopical lattice.

The finite difference numerical method is applied in all the calculations, and a uniform mesh is used (with 1000 × 1000 grid points). The physical parameters of Ni–Cu alloy consult Refs. [1, 19], and the following parameters keep fixed: $\mathrm{N}_X = \mathrm{N}_Y = 1000$, $\mathrm{HN}_X = \mathrm{HN}_Y = 100$, $\sigma^\mathrm{A} = 3.7 \times 10^{-5}$ J/cm^2, $\sigma^\mathrm{B} = 2.9 \times 10^{-5}$ J/cm^2, $D_\mathrm{L} = 1.0 \times 10^{-5}$ cm^2/s, $D_\mathrm{S} = 1.0 \times 10^{-9}$ cm^2/s, $D_T = 2.0 \times 10^{-3}$ cm^2/s; $v_\mathrm{m} = 7.42$ cm^3/mol, $L_\mathrm{A} = 2350$ J/cm^3, $L_\mathrm{B} = 1728$ J/cm^3, $R_\mathrm{g} = 8.314$ J/mol, $\beta^\mathrm{A} = 0.33$, $\beta^\mathrm{B} = 0.39$, $\gamma = 0.04$, $k = 4$, $\Delta x = 3.0 \times 10^{-6}$ cm, $\Delta t = (\Delta x)^2/5D_\mathrm{L}$, $\delta_\mathrm{A} = \Delta x/0.8$, $\delta_\mathrm{B} = \Delta x/0.63$, $T_\mathrm{m}^\mathrm{A} = 1728$ K, $T_\mathrm{m}^\mathrm{B} = 1358$ K, $\bar{A} = 0.01$. N_X and N_Y are microscopic lattice numbers of X and Y axes. HN_X and HN_Y are macroscopical lattice numbers of X and Y axes. The initial concentrations of the melt, $C_0 = 0.4083$ (at.%Cu), and the initial temperature, $T_0 = 1574$, are chosen. The zero-Neumann boundary conditions for Φ and c are imposed at the boundaries of the computational domain, and described by $\partial\Phi/\partial n = 0$, $\partial c/\partial n = 0$. However, the boundary with different heat fluxes is chosen in the temperature-field calculation. There is a heat flux on the left boundary, which is described by $Q = \lambda \partial T/\partial n$. The other three boundaries are imposed zero-Neumann boundary condition. At the initial time, two crystal nuclei are seeded in the left of the calculating zone, and the central coordinates are (0, 200) and (0, 800).

Results and discussion

Growth of the crystal

As we know, heat flux has much to do with the microstructure of directional solidification, and this study discussed the evolution of dendritic growth with different heat fluxes. In the calculating zone, only the left boundary is imposed steady heat flux, and the other three boundaries have no heat flow.

Firstly, the heat flux is set to 18 W/cm^2, which is a lower heat flow. Figure 1 shows the evolutionary process with four pictures of directional solidification. In the simulations below, those arms growing parallel to *X*-axis are called the transverse side branches and those parallel to *Y*-axis are called the lengthways side branches. As shown in Fig. 1a, two crystal nuclei, which are seeded in the left of the calculating domain, begin to grow. There is a higher condensate depression at the left boundary because of heat flow and heat diffusion, so the dendritic growth in the left zone grows much quicker. There is a stochastic disturbance at the interface of solid and liquid phases and many secondary arms appear. The competitive growth of transverse side branch and the lengthways side branch is very important to the microstructure of directional solidification before the tree-like crystal goes steadily. Transverse steady heat flux and heat diffusion are the main power of the transverse dendritic growth, and the initial undercooling and heat diffusion are the main power of the lengthways side branch. Figure 1b and c shows the competitive process of transverse side branches and lengthways side branches before the steady growth. In the initial stage, the latent heat released is less because the crystal nuclei are too small. However, the latent heat released increases gradually along with the growth of crystal grain. The temperature field and gradient in front of the interface are the main factors in the non-isothermal solidification. Because of the heat flux is very small, the latent heat cannot release in time through

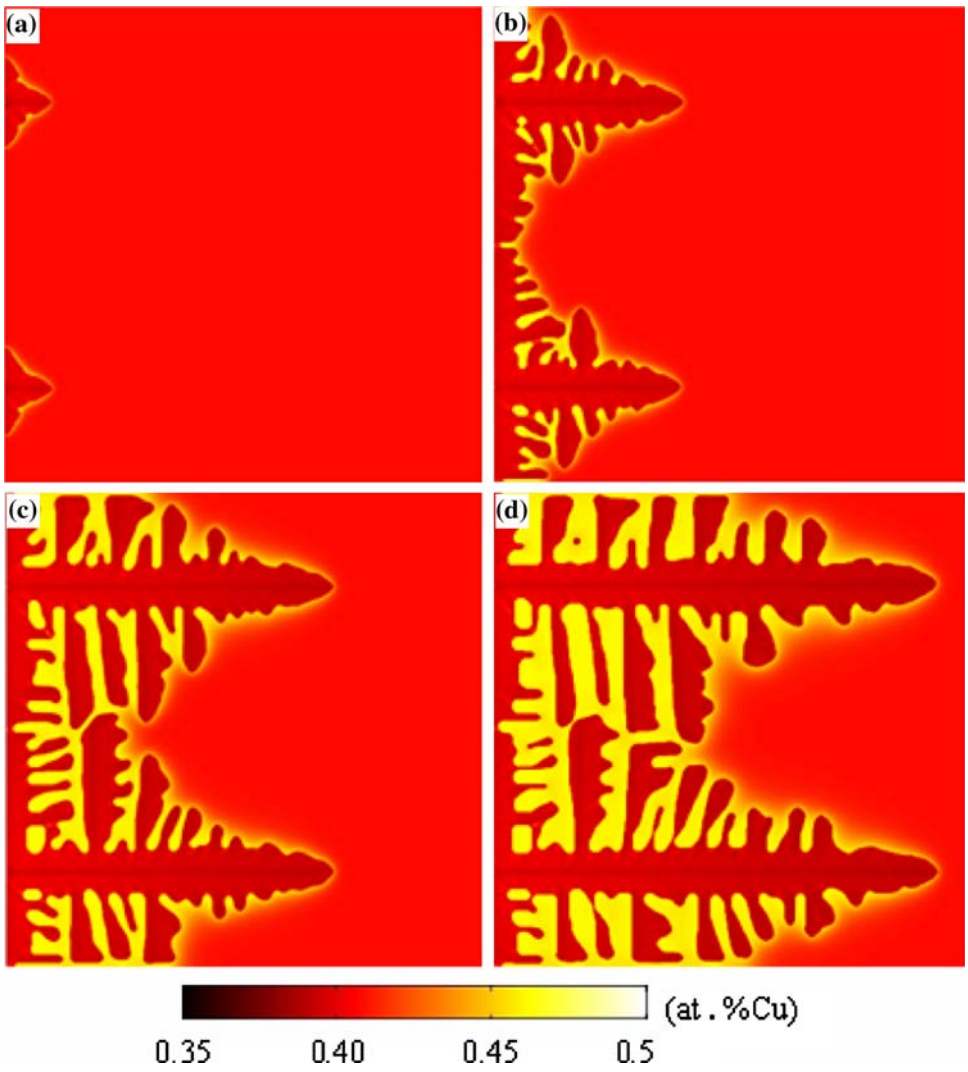

Fig. 1 Evolution process of directional solidification with the left boundary heat flux equal to 18 W/cm^2. **a** $t = 0.2046$ ms, **b** $t = 1.0230$ ms, **c** $t = 2.2506$ ms, and **d** $t = 3.6828$ ms

the left boundary. Therefore the growth of transverse side branches is restrained. However, the growth of lengthways side branches is quicker than the transverse ones because of the initial overcooling. As shown in Fig. 1c, when the lengthways secondary arms once grow bigger, the freezing latent heat and solute diffuseness will further restrain the growth of the transverse side branches. Figure 1d shows the final result of competitive growth, and it can be clearly seen that the transverse side branches are restrained by the lengthways secondary arms. There is a much thicker solute boundary layer between the arms. At the same time, the temperature is higher in the freezing zone, where arms are competitively growing. All these factors result in dendritic arms to remelt, and this can be seen in Fig. 1d. This evolution process also show the conversion process from dendritic crystal to columnar crystals.

Secondly, we investigate the directional solidification with a little stronger heat flux, say 36 W/cm^2. The calculated result is shown in Fig. 2. Figure 2a shows that two crystal nuclei begin to grow and there is little difference when compared with Fig. 1a. At 0.8184 ms, transverse arms and lengthways arms begin to grow competitively, which is shown in Fig. 2b and c. Because of the steady heat flux at the left boundary, the latent heat is released in time. This affords a certain power to the growth of transverse arms. At the same time, the initial supercooling in front of the interface also gives much power to the growth of lengthways arms. In this way, the competitive growth of two directional dendritic arms appears. As shown in Fig. 2b and c, the dendritic crystals gradually become columnar crystals with the steady heat flow at the left boundary. Figure 2d shows the final growth of columnar crystals. It can also be seen that there is thick solute layer in the arms, and the arms between the two columnar crystals grow completely and restrain each other. At the same time, there is obvious tertiary arms emergence in the calculation zone. Thereby, transverse side branches and lengthways side branches coexist when the heat flux equal to 36 W/cm^2.

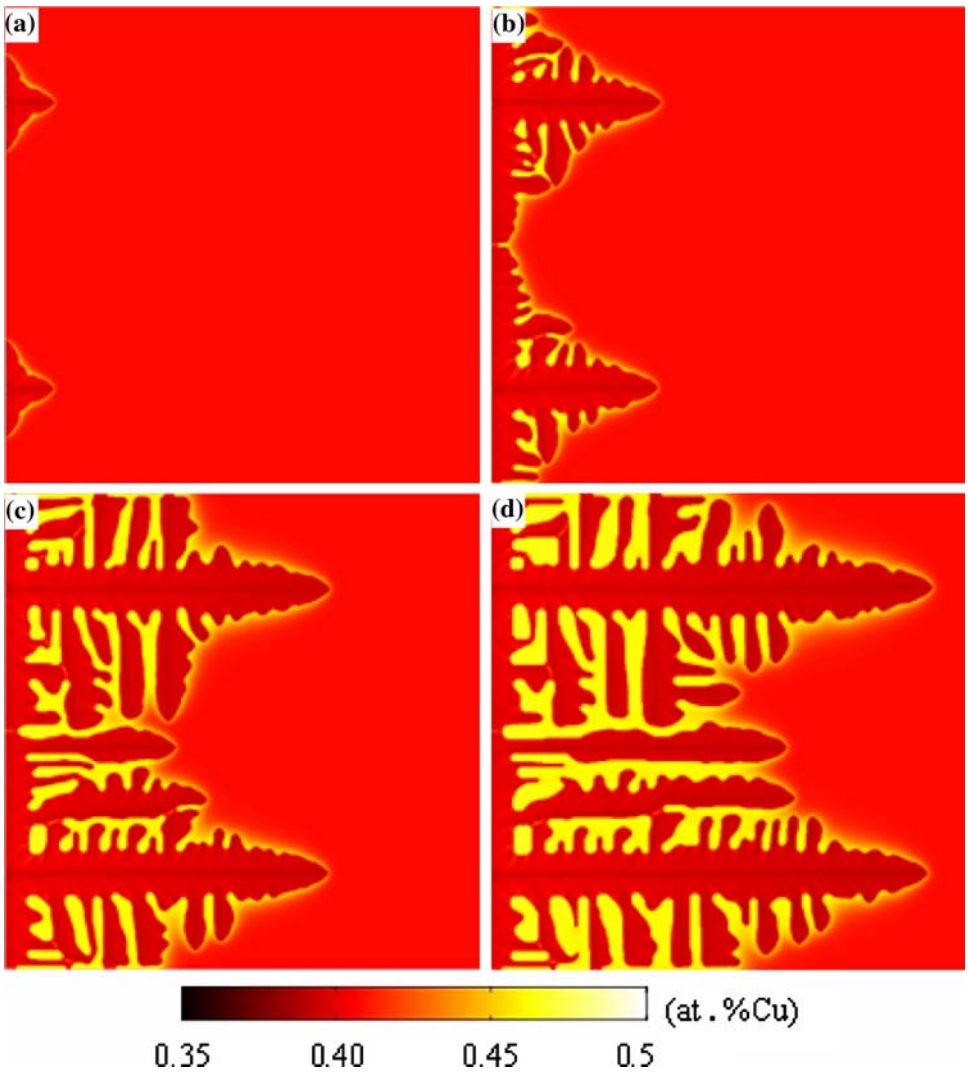

Fig. 2 Evolution process of directional solidification with the left boundary heat flux equal to 36 W/cm^2. **a** $t = 0.2046$ ms, **b** $t = 0.8184$ ms, **c** $t = 1.9096$ ms, and **d** $t = 2.9326$ ms

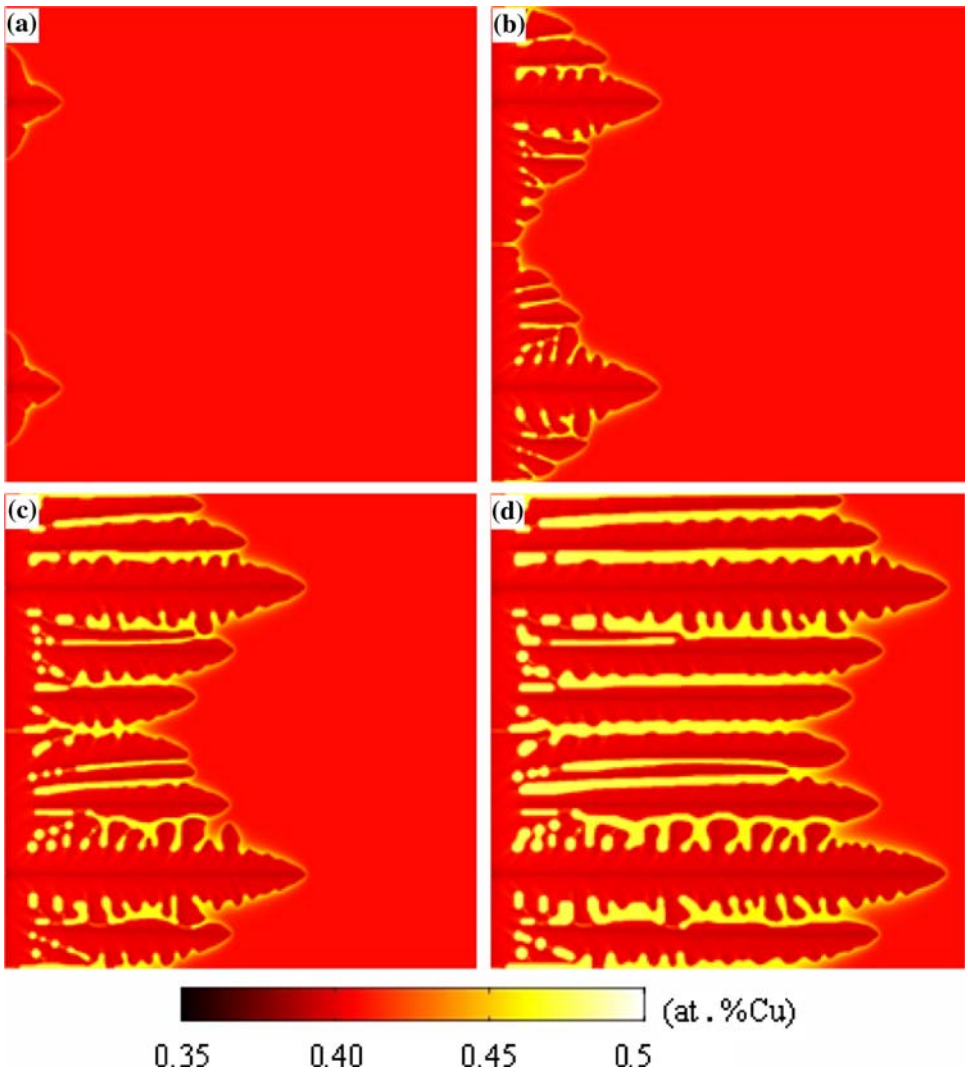

Fig. 3 Evolution process of directional solidification with the left boundary heat flux equal to 90 W/cm^2. **a** $t = 0.2046$ ms, **b** $t = 0.6820$ ms, **c** $t = 1.3640$ ms, and **d** $t = 2.3188$ ms

Thirdly, Fig. 3 shows the evolution process of directional solidification with the heat flux equal to 90 W/cm^2. In this simulation, the heat flow is set much higher, and the transverse diffuseness of heat flow takes the leading place. Figure 3a shows when the two crystal nuclei grow for 0.2046 ms. Because of the higher steady heat flow and the undercooling, the crystal nuclei gradually develop into dendritic crystal. The transverse heat flux is much higher, so the transverse arms have predominance and grow firstly. Figure 3b and c shows that the growth of lengthways arms are controlled by the transverse priority growth because the transverse growth releases much latent heat and solute. Figure 3b and c shows also the conversion process from dendritic crystals to columnar crystals. The spacing of columnar crystals is smaller than that of Fig. 1. Because of the quicker rate of growth, the solute in front of the interface has less time to diffuse, and the microsegregation is higher than that of Fig. 1. Figure 3d shows the final growth of columnar crystals. It can be seen from the figure that the growth of columnar crystals is also a process of competition and selection, and the preferential columnar crystals completely grow with the initial columnar crystals. The steady heat flow of boundary layer is the dynamic force of columnar crystals growth. In this way, the higher heat flow speeds up the invert speed of columnar crystals.

Lastly, in order to obtain the directional solidification with the biggest heat flow, we set it to 180 W/cm^2. Figure 4 shows the evolution process. Because of the high heat flow, the latent heat of phase transition has little effect on the dendritic growth. The transverse heat diffusion makes much higher temperature gradient for the transverse arms growth in front of the interface, so the rate of growth is high. From Fig. 4a, it can be seen that the growth of crystal nuclei is quicker than any one above at the same growing time. Figure 4b and c shows the competitive growing process of columnar crystals. In this section, the transverse small columnar crystals are produced straightway by the interface disturbance, and they competitively

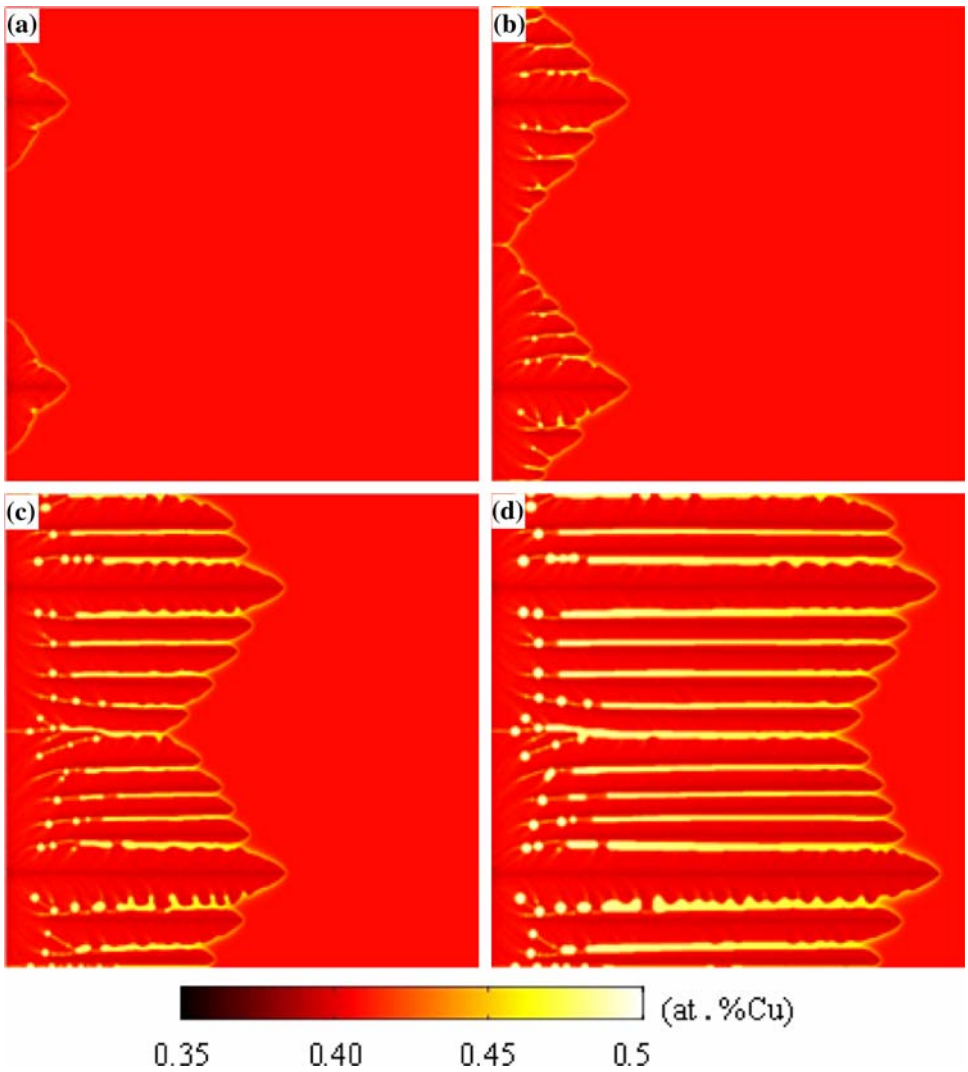

Fig. 4 Evolution process of directional solidification with the left boundary heat flux equal to 180 W/cm^2.
a $t = 0.2046$ ms,
b $t = 0.4774$ ms,
c $t = 1.0230$ ms, and
d $t = 1.7732$ ms

grow with the initial columnar crystals. The spacing of columnar crystals changes continually and gradually becomes identical. The microsegregation is the most serious because of the biggest growing velocity. Figure 4d shows the final microstructure of directional solidification.

Calculational data

The temperature field plays a very important role in non-isothermal solidification, so we first analyze the temperature distribution and varieties in the calculational zone. In order to explain the problem expediently, we set the simulation with heat flow equal to 18 W/cm^2 to Sim 1, and so on. Figure 5a and b shows the highest and lowest temperatures at arbitrary time with different heat fluxes. The highest temperature is general in the interface, where the phase transition takes place and the latent heat is released. However, the location of the lowest temperature has two likelihoods. If the heat flux is small, 18 W/cm^2 for example, the latent heat of phase transition cannot be completely released through the left boundary. The temperature of the calculational zone increases gradually with the time running out. In this way, the location of the lowest temperature is in the undercooling liquid phase far from the interface in the initial stage. However, in the last stage the location is in the left boundary layer. The reason is that the temperature of liquid phase increases high enough, and phase transition occurs slowly. At this time, the heat quantity has no choice but to release through the left boundary layer. From Fig. 5, it can be seen that the curves of the highest and lowest temperatures versus time change variously with different heat flow. The highest temperature of Sim 1 is higher than that of others at any time, and the highest temperature of Sim 2 is a little lower than that of Sim 1. The highest temperature of Sim 3 and Sim 4 is the initial temperature in the initial stage, because the latent heat is released from boundary in time. However, some parts in the calculational zone are overheated in the last stage because the fraction of solid phase

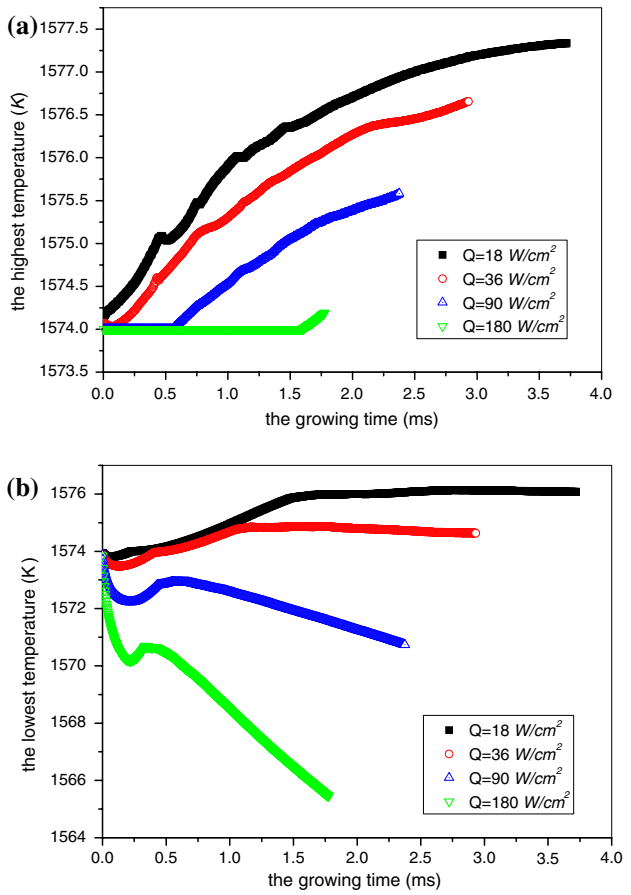

Fig. 5 The highest and the lowest temperatures versus time: **a** the highest temperature versus time; **b** the lowest temperature versus time

and freezing distance increase. The lowest temperatures of Sim 1 and Sim 2 increase in the initial stage, and become stable in the last stage. Nevertheless, the stable temperature of Sim 2 is lower than that of Sim 1. The lowest temperatures of Sim 3 and Sim 4 decrease in the initial stage, increase in the middle stage, and continue to decrease in the last stage. In the initial stage, the fraction of solid phase is small, the temperature decreases gradually. With the fraction of solid phase increasing, the curve of the lowest temperature has a small wave crest in the middle stage. With the freezing distance increasing, the latent heat cannot be released from the left boundary in time, and the temperature continues to decrease in the last stage.

Table 1 gives the calculated results of different heat fluxes. It can be seen that the higher the heat flux is, the smaller the growing time is, and the quicker the average growing rate is. The latent heat is released in time with higher heat flow and the growth of columnar crystals is accelerated. Table 1 also gives the data of microsegregation. The ratio of segregation is the data that the biggest concentration divided by the smallest concentration in the calculational zone at given time. The ratio of segregation increases gradually with the increase in heat flux. If the heat flux is smaller, the velocity of dendritic growth is smaller and the solute of liquid phase has enough time to diffuse. So the ratio of segregation is smaller. However, if the heat flux is higher, the columnar crystals grow so quickly that the solute has no enough time to diffuse. In the next place, the temperature is lower in the left boundary zone because of the higher heat flux, the supersaturation enhances, and the ratio of segregation increases. Lastly, the grown columnar crystals hold back the interdendritic solute diffusion, and the concentration between the columnar crystals is higher. As given in Table 1, the average spacing of columnar crystals becomes small with the heat flux increasing. If the heat flux is small, the latent heat of phase transition reduces the feasibility that the columnar crystals come into being and grow up. With big heat flux, the talent heat is released in time through the boundary. The big supercooling and temperature gradient accelerate the growth of columnar crystals.

In order to study temperature distribution further, the macroscopical temperature field is anatomized along dendritic trunk and the position of cross section is shown in Fig. 6. The temperature data of dendritic trunk are given in Fig. 7. Figure 6 shows the macroscopical temperature field of Sim 1 at 0.8184 ms. From the figure, it can be seen that the temperature is higher where the phase transition takes place. Figure 7 shows the data from Sim 1 to Sim 4 each at four slices. Figure 7a shows the data of Sim 1. From the figure, it can be seen that the temperature at the left boundary increases quickly in the initial stage, and changes a little when the temperature becomes stable in the last stage. Because of adiabatic boundary condition, the liquid-phase temperature in the right zone increases all the time and reaches about 1577.3 K at 3.6828 ms. Figure 7b shows the

Table 1 Calculated results of different rates of heat flow

	Sim 1	Sim 2	Sim 3	Sim 4
Heat flux (W/cm^2)	18	36	90	180
Growing time (ms)	3.6828	2.9326	2.3188	1.7732
Average growing rate (cm/s)	0.7603	0.9548	1.2075	1.5791
Ratio of segregation	1.238	1.241	1.263	1.290
The average spacing of columnar crystals (cm)	0.168	0.072	0.034	0.018

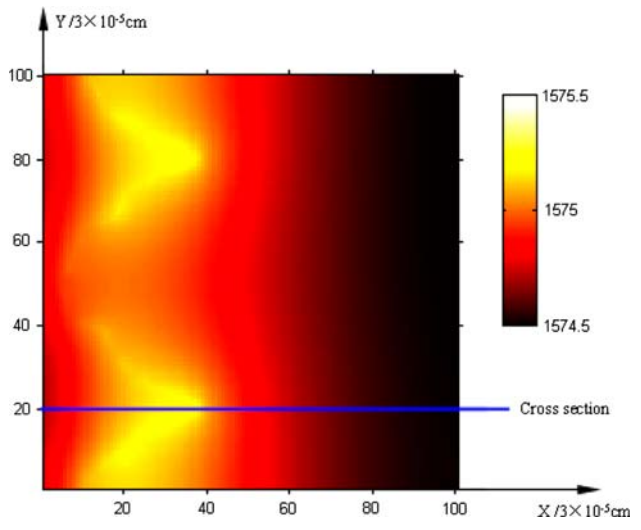

Fig. 6 The abridged general view of cross section and the macroscopical temperature field with the heat flux equal to 36 W/cm^2 at 0.8184 ms

data of Sim 2. The temperature at left boundary increases quickly in initial stage too, and a little falls in the last stage. The higher temperature of liquid phase decreases the ratio of phase transition and the temperature gradient increases. So the temperature of left boundary has a slightly fall in the last stage. Figure 7c and d shows the temperature distribution of dendritic main trunk with higher heat flux. As shown in Fig. 7c, the temperature of left boundary changes a little in the initial stage, and gradually falls in the last stage. The temperature of liquid phase decreases slightly, and increases gradually in the last stage. Figure 7d shows the result of the highest heat flux. From the four slice curves, it can be seen that the latent heat is released through the boundary in time, and there is little heat quantity accumulated in the liquid phase. The temperature of left boundary decreases gradually, and reaches 1565.5 K at 1.7732 ms. The temperature of liquid phase changes a little, about only 1 K. As a whole, the solid temperature gradient of dendritic main trunk is different with different heat fluxes when the growth of dendritic crystal is stable. The solid temperature gradients from Sim 1 to Sim 2 are, respectively, 0.50×10^{-3} K/cm, 0.83×10^{-3} K/cm, 1.70×10^{-3} K/cm, and 3.10×10^{-3} K/cm. The higher the heat flux is, and the higher the solid temperature gradient of dendritic main trunk is.

Conclusion

The heat flux does much to the growth of dendritic crystal. The growth manner is dendritic crystals with the lower heat

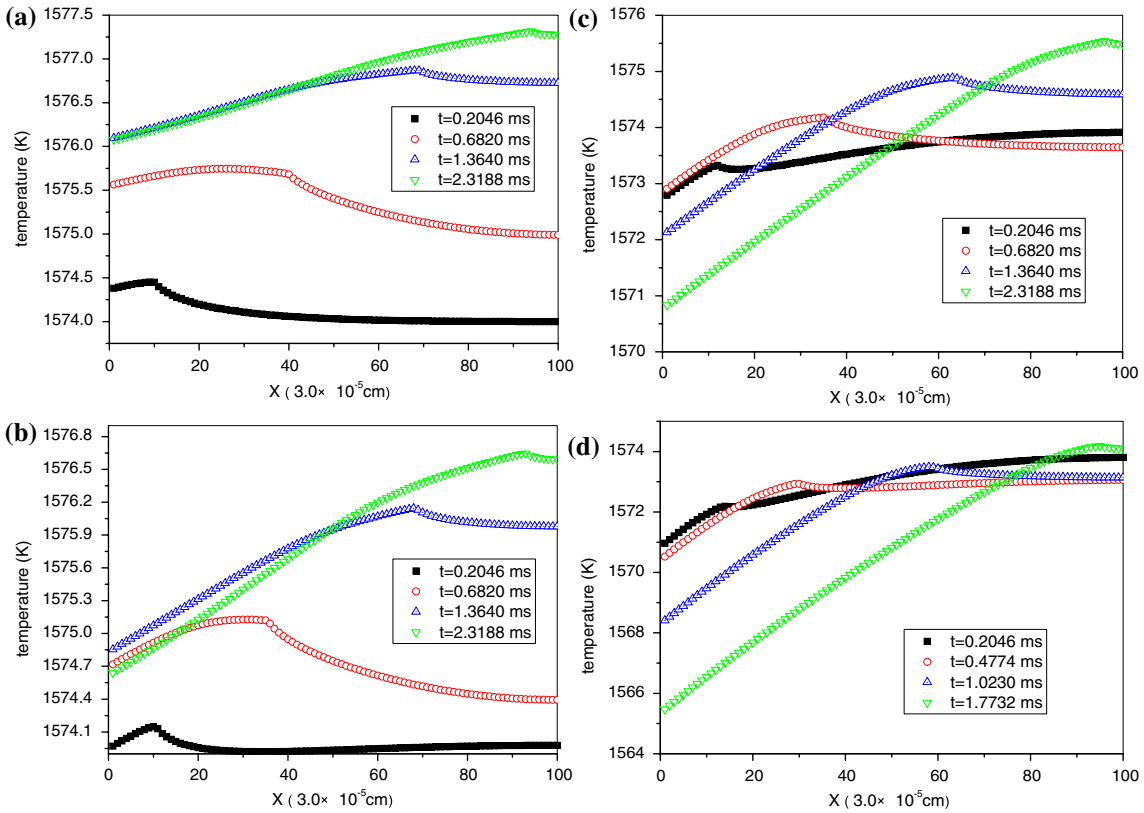

Fig. 7 The cross-sectional temperatures of dendritic main arbor at special times with different boundary heat fluxes. **a** 18 W/cm^2; **b** 36 W/cm^2; **c** 90 W/cm^2; **d** 180 W/cm^2

flux, and the growth manner is columnar crystals with the higher heat flux. The big heat flux changes the growth manner from dendritic crystals to columnar crystals. When the heat flow equal to 18 W/cm^2, the growth of lengthways arms is accelerated, and the growth of columnar crystals is restrained. When the heat flow equal to 36 W/cm^2, the lengthways arms and transverse arms grow completely. When the heat flow equal to 90 W/cm^2, the lengthways growth is restrained, and the growth of columnar crystals is priority. When the heat flow equal to 180 W/cm^2, the columnar crystals change into the thinner columnar crystals. At the same time, the higher the heat flux is, the quicker the growing velocity is, the higher the ratio of segregation is, and the smaller the average spacing of columnar crystals is.

The heat flux also plays an important role in microscopic temperature distribution. Microscopic temperature field has much contribution to the growth of dendritic crystal in non-isothermal solidification. The temperature in the zone of phase transition is higher, and the growth of dendritic crystals is along the direction in which the temperature gradient is the biggest. The highest temperature gradually increases with lower heat flux, but the highest temperature keeps changeless for a long time with higher heat flux. With lower heat flux, the lowest temperature increases gradually in the initial stage, and changes a little in the last stage. With higher heat flux, the lowest temperature falls immediately, has a wave, and continues to fall. From the cross-sectional temperature of dendritic main trunk, it can be seen that with lower heat flux, the temperature on the left boundary and the temperature in the right liquid phase both increase, and the temperature contrast is smaller. With higher heat flux, the temperature on the left boundary decreases gradually and the temperature in the right liquid phase changes a little. The temperature contrast is higher. At the same time, the solid temperature gradients of dendritic main trunk are different with different heat fluxes when the growth of dendritic crystal is stable. The higher the heat flux is, and the higher the solid temperature gradient of dendritic main trunk is.

References

1. Wheeler AA, Boettinger WJ, McFadden GB (1992) Phys Rev A 45:7424
2. Wheeler AA, Boettinger WJ, McFadden GB (1993) Phys Rev E 47:1893
3. Boettinger WJ, Warren JA (1996) Metall Mater Trans A 27:657
4. Warren JA, Boettinger WJ (1995) Acta Metall Mater 43:689
5. Boettinger WJ, Warren JA (1999) J Cryst Growth 200:583
6. Kim SG, Kim WT, Suzuki T (1999) Phys Rev E 60:7186
7. Kim SG, Kim WT, Suzuki T (1998) Phys Rev E 58:3316
8. Boettinger WJ, Warren JA, Beckermann C, Karma A (2002) Annu Rev Mater Sci 32:163
9. Kim SG, Kim WT (2001) Mater Sci Eng A Structure 304–306:281
10. Diepers H-J, Ma D, Steinbach I (2002) J Cryst Growth 237–239:149
11. Bi Z, Sekerka RF (2002) J Cryst Growth 237–239:138
12. Guo JJ, Li XZ, Su YQ, Wu SP, Li BS, Fu HZ (2004) Rare Met Mater Eng 33:195
13. Costa Filho RN, Kosterlitz JM, Granato E (2005) Physica A 354:333
14. Lan CW, Chang YC (2003) J Cryst Growth 250:525
15. Lan CW, Shih CJ, Lee MH (2005) Acta Mater 53:2285
16. Lan CW, Lee MH, Chuang MH, Shih CJ (2006) J Cryst Growth 295:202
17. Singer HM, Singer-Loginova I, Bilgram JH, Amberg G (2006) J Cryst Growth 296:58
18. Plapp M (2007) J Cryst Growth 303:49
19. McCarthy JF (1997) Acta Mater 45:4077